

# Protostellar Evolution during Time Dependent, Anisotropic Collapse

Mahmoud Aburihan<sup>1</sup> <sup>★</sup>, Jason D. Fiege<sup>2</sup> <sup>†</sup>, Richard N. Henriksen<sup>1</sup> <sup>‡</sup>, and Thibaut Lery<sup>3</sup> <sup>§</sup>

<sup>1</sup>Queen's University, Kingston, Ontario, Canada

<sup>2</sup>Canadian Institute for Theoretical Astrophysics, McLennan Labs, University of Toronto 60 St. George Street, Toronto, Ontario, M5S 3H8

<sup>3</sup>DIAS, School of Cosmic Physics, 5 Merrion Square, Dublin 2 Ireland

8 November 2018

## ABSTRACT

The formation and collapse of a protostar involves the simultaneous infall and outflow of material in the presence of magnetic fields, self-gravity, and rotation. We use self-similar techniques to self-consistently model the anisotropic collapse and outflow by a set of angle-separated self-similar equations. The outflow is quite strong in our model, with the velocity increasing in proportion to radius, and material formally escaping to infinity in the finite time required for the central singularity to develop.

Analytically tractable collapse models have been limited mainly to spherically symmetric collapse, with neither magnetic field nor rotation. Other analyses usually employ extensive numerical simulations, or either perturbative or quasistatic techniques. Our model is unique as an exact solution to the non-stationary equations of self-gravitating MHD, which features co-existing regions of infall and outflow.

The velocity and magnetic topology of our model is quadrupolar, although dipolar solutions may also exist. We provide a qualitative model for the origin and subsequent evolution of such a state. However, a central singularity forms at late times, and we expect the late time behaviour to be dominated by the singularity rather than to depend on the details of its initial state. Our solution may, therefore, have the character of an attractor among a much more general class of self-similarity.

**Key words:** stars: formation–MHD–ISM: magnetic fields–ISM: clouds

## 1 INTRODUCTION

It is clear that outflows often co-exist with infall as protostars form within the collapsing cores of molecular clouds (Bertout 1989; André *et al.* 1993). Infall and outflow both appear to be present for much of the protostellar “main sequence,” from rapidly accreting embedded Class 0 objects to fully formed T Tauri stars. This suggests that the dynamics leading to the formation of a protostar are more complex than simple radial infall, and are dominated by strongly anisotropic motions. We present a new model for the anisotropic collapse of a molecular cloud core, which self-consistently treats the effects due to self-gravity, magnetic

fields, and rotation, as the central protostellar core grows and a bipolar outflow develops.

Self-gravitating models of protostellar collapse have usually been limited to the classical solutions with spherical symmetry (Larson, 1969; Penston, 1969; Shu, 1977), including the elaborations and clarifications in related works (Hunter, 1977; Whitworth and Summers, 1985; Henriksen, André and Bontemps, 1997, hereafter HAB1997). Galli and Shu (1993, hereafter GS) presented a very interesting calculation, which included the effects of anisotropy as a perturbation about the classical Shu (1977) inside-out collapse solution. Subsequently, Li and Shu (1996) presented a quasi-static calculation. An approximate analytic self-similar treatment based on a dynamic termination of the ambipolar diffusion models has also been given recently and developed to the point of comparison with observations (e.g. Basu, 1997). However the bipolar outflow was not integral to any of these papers, as it is in the case of the present work.

We have previously studied steady-state solutions for simultaneous infall and outflow late in the evolutionary sequence, after the dominant central mass had already formed

<sup>★</sup> This paper developed from an insightful MSc. thesis by Mahmoud Aburihan whose accidental death on Dec. 20, 1999 is greatly regretted by his colleagues and many friends. His co-authors would like to dedicate this work to his memory and to his family.

<sup>†</sup> fiege@cita.utoronto.ca

<sup>‡</sup> henriksn@astro.queensu.ca

<sup>§</sup> lery@cp.dias.ie

(Henriksen and Valls-Gabaud, 1994; Fiege & Henriksen 1996, hereafter FH1; Lery, Henriksen, & Fiege 1999, hereafter LHF). Thus, our previous models apply only to very late times in the formation of a protostar. The philosophy of these articles was that bipolarity could be studied using scale free solutions near the central singularity without worrying too much about the initial state of the flow. This is similar in spirit to the development of the Larson-Penston self-similar solution from non-self-similar initial conditions.

The model presented in this paper takes quite a different approach by treating the time-dependent problem of accretion and simultaneous outflow in a dynamically collapsing and self-gravitating core. Thus, we study an early stage of stellar formation when the star has not yet formed, and most of the gas still resides in the surroundings. A limit to the self-gravitating regime is certainly set when the mass of the central object dominates that of the surroundings. Thus our present solution is a natural complement to our earlier studies.

The present model is best described as an inner “settling” solution, which follows the assembly of the protostar in detail. It is limited to smaller spatial scales than our previous work, but the flow structure that we predict would presumably be embedded within a larger collapsing region. This larger region might include nearly steady-state outflows and an accretion region of the self-similar type that we have previously discussed in FH1 and LHF (See Section 5).

Numerical simulations have also been used to study non-isotropic self-gravitating collapse. For example, Tomisaka (1998) used a multi-grid MHD code to study the gravitational collapse of a segment of a magnetized and slowly rotating filament. His simulation resulted in a rotating pseudo-disc, which produced an outflow as the central object grew. Most interesting, from our point of view, is that the late stages of the calculation were dominated by a quadrupolar velocity field. Such quadrupolarity can develop in super-Alfvénic flows when infalling material near the midplane is deflected up the axis due to a combination of pressure gradients, magnetic fields, and the centrifugal barrier. Our present calculation shows that this mechanism can operate on smaller scales between the growing boundary of the hydrostatic core and the pressure dominated region external to the region of self-similarity. The development of quadrupolar structure and the connection of our model to the exterior region is discussed in Section 5.

Our central assumption is that this early stage of star formation is dynamic rather than quasi-static. This is suggested by various lines of evidence (Basu, 1997; Foster and Chevalier, 1993; HAB, 1997), although this assumption cannot be regarded as certain (Basu and Mouschovias 1995a; Basu and Mouschovias 1995b; Galli and Shu, 1993; Li and Shu, 1997). In any case, the central regions must ultimately become hydrostatic to allow for the growth of the naissant protostar. Thus, we expect and do indeed find “settling” solutions, in which the radial velocity goes to zero near the centre, where the infalling material actually forms the stellar core.

In the following section, we derive our basic self-similar equations from self-gravitating MHD, under the assumption of self-similar flow. We show, in Section 4, that our equations admit an exact and completely analytic class of solutions. We use these solutions to derive several interesting analytic

results, which illustrate and constrain the properties of the model. Our most important result is that substantial outflow velocities can be obtained without resorting to heating the material, as in FH1 and LHF. The axial outflow velocity is never more than twice the equatorial inflow velocity on a sphere of some given radius, at some instant of time. However, we find that the outflow velocity increases linearly with distance, so that substantial velocities are obtained far from the origin. By following the motion of individual fluid elements, we find that all such fluid elements escape to radial infinity in the finite time required for the central singularity to develop. This escaping gas would presumably interact with the external medium in a complicated manner, which we discuss in Section 5. Our Discussion section also presents a simple, qualitative model to provide one possible way in which the quadrupolar structure might arise. We also note that models with dipolar geometry are also possible, although we do not find them explicitly in the present calculation.

Finally, we note that a preliminary account of this work was presented at the Cracow meeting on “Plasma Turbulence and Energetic Particles in Astrophysics” (1999, M. Ostrowski and R. Schlickeiser, eds.).

## 2 SELF-SIMILAR ACCRETION AND OUTFLOW

We assume that the protostellar development begins with the primarily radial collapse of a cold molecular core. In reality, cores are not really expected to be spherical (Tomisaka *et al.* 1988, Myers *et al.* 1991, Ryden 1996, Fiege & Pudritz 2000a), but all that is really required is that there be a substantial collapse in a plane perpendicular to the initial magnetic and rotation axes (assumed to be parallel for simplicity). The core may have been in equilibrium initially as a singular isothermal sphere (SIS) as in GS, or it may have had a more complicated internal structure as suggested by HAB. The initial conditions provide a set of characteristic scales, which suggest the set of conserved quantities used to define the class of self-similar symmetry. For example, the obvious constants for an unbounded SIS are the sound speed  $c_s$  and Newton’s constant  $G$ . GS used these constants to define a “class” of self-similarity obeyed during the collapse. On the other hand, a constant external pressure bounding a truncated self-gravitating sphere, together with  $G$ , would define a different class of self-similarity. Yet another similarity class would be appropriate if there were a characteristic time due to rotation.

Carter and Henriksen (1991) developed a mathematical formalism for determining the most general class of self-similarity possible, which naturally includes all possible initial states. This method has been used successfully in studying the evolution of collisionless n-body systems (see e.g. Henriksen, 1997), but is equally well-suited for studying the dynamical collapse of a magnetized, self-gravitating core. This technique can be used to demonstrate the existence of the separable (in radius, poloidal angle, and time) “settling” solution presented here, as a special case within a more general class of self-similarity. It is possible that these separable solution might represent an “attractor” within this

larger class of self-similar models (Aburhan, 1999), but we do not prove this here.

It is important to address the question of how the quadrupolar magnetic and flow structure assumed by our model might originate. Such questions are really beyond the scope of our self-similar treatment, since self-similar solutions are often *intermediate*, in the sense that they are disconnected from their boundary conditions in space or time (see discussion in FH1). Thus, our ideas regarding the origin of our self-similar model are somewhat speculative. Nevertheless, we suggest a reasonable scenario in Section 5, by which a rotating and magnetized cloud could evolve a quadrupolar flow and magnetic field structure during collapse. This would arise as a consequence of poloidal pressure gradients, the centrifugal barrier encountered by the collapsing cloud, and magnetic reconnection effects which change the topology of the field in regions where localized field reversals occur. We discuss the details of this scenario in Section 5, and turn now to a derivation of the basic equations.

## 2.1 Equations

The basic non-dimensional quantities from which we construct our self-similar model are given by the poloidal angle  $\theta$  and the variable

$$X \equiv -\frac{r}{c_s t}, \quad (1)$$

where  $r$  is spherical radius,  $t$  is time, and  $c_s$  is a *fiducial* sound speed. The local sound speed need not be constant; the constant  $c_s$  in equation 1 is only meant to be typical of the initial conditions. The minus sign is included to make  $X$  positive definite, since our model starts with  $t$  large and negative, evolving toward a singularity at  $t = 0$ . Note that our  $X$  is essentially the same as the self-similar variable used by Shu (1977) and more recently by GS in the context of collapsing isothermal spheres, although their model is strictly isothermal. We provide a self-similar framework in this section which would, in principle, allow one to follow the collapse of a SIS.

Our treatment admits considerable freedom in choosing the equation of state (EOS). One particularly simple non-isothermal choice, which we discuss later in this section and use extensively throughout this paper, makes the partial differential equations separable, which allows us to find a singular and completely analytic solution to our self-similar equations. Unfortunately, this particular solution does not match on to the SIS at early times. A more complete treatment of the collapse problem would solve (with greater effort) the general self-similar PDEs directly, beginning with realistic initial conditions, such as a SIS threaded by a magnetic field, rather than seeking out special separable forms. However, our singular solution might represent an “attractor” among the more general class of self-similarity, which would make it a valid end state for a wide variety of initial conditions. This possibility is further explored in Section 5.

The actual temperature and sound speed in our model vary as functions of  $r$ ,  $\theta$ , and  $t$  in a way that is uniquely determined by the self-similarity. Generally speaking, the gas heats up during collapse in our model, although with significant temperature structure in  $\theta$ . Isothermality in cores

is maintained primarily by the efficient cooling provided by molecular lines. An anisotropically collapsing core would likely evolve toward a more complex temperature structure once the dynamical timescale  $r/c_s$  becomes shorter than the cooling time. Thus, we expect the self-similarity to develop from the inside out, with the central regions of the collapsing core evolving more rapidly toward a self-similar flow pattern, while the outer layers remain nearly isothermal until later in the collapse.

The most general class of self-similarity based on  $X$  and  $\theta$  is expressed by writing all physical quantities as functions of these variables:

$$\rho = \frac{c_s^2}{4\pi G r^2} \bar{\mu}(X, \theta) \quad (2)$$

$$\mathbf{v} = c_s \bar{\mathbf{W}}(X, \theta) \quad (3)$$

$$\mathbf{B} = \sqrt{\frac{c_s^4}{G}} \frac{\bar{\mathbf{b}}(X, \theta)}{r} \quad (4)$$

$$\Phi = c_s^2 \bar{\psi}(X, \theta) \quad (5)$$

$$P = \frac{c_s^4}{4\pi G} \left( \frac{p_0(t)}{r_0^2} + \frac{\bar{p}(X, \theta)}{r^2} \right). \quad (6)$$

The notation for the dimensional magnetohydrodynamic (MHD) quantities on the left hand side of these equations is standard, and the quantities  $\bar{\mu}$ ,  $\bar{\mathbf{W}}$ ,  $\bar{\mathbf{b}}$ ,  $\bar{\psi}$ , and  $\bar{p}$  on the right hand side are dimensionless forms of the density, velocity, magnetic field, gravitational potential, and “dynamical” pressure respectively. Note that we separate the pressure into a “dynamical” pressure term  $\bar{p}$ , and a background pressure term  $p_0(t)$ . The term involving  $p_0(t)$  has no dynamical consequences whatsoever, since it does not contribute to the pressure gradient. It is necessary because realistic solutions are obtained only when the “dynamical” part of the pressure  $\bar{p} < 0$ , as we shall further discuss in Section 4.1. Finally, note that the overbars distinguish these quantities from the separated forms of these variables, presented later in this section.

We now use the preceding ansatz of self-similarity in each of the equations of self-gravitating MHD to obtain our general set of self-similar equations. Poisson’s equation, the continuity equation, and the condition that there are no magnetic monopoles are written respectively as follows:

### Poisson’s Equation

$$X^2 \partial_X^2 \bar{\psi} + 2X \partial_X \bar{\psi} + \frac{1}{\sin \theta} \partial_\theta (\sin \theta \partial_\theta \bar{\psi}) = \bar{\mu}; \quad (7)$$

### Continuity

$$(\bar{W}_r + X) X \partial_X \bar{\mu} + \bar{\mu} X \partial_X \bar{W}_r + \frac{1}{\sin \theta} \partial_\theta (\bar{\mu} \bar{W}_\theta \sin \theta) = 0; \quad (8)$$

### No Magnetic Poles

$$\partial_X (X \bar{b}_r) + \frac{1}{\sin \theta} \partial_\theta (\sin \theta \bar{b}_\theta) = 0. \quad (9)$$

The 3 components of the MHD induction equation are given by the following:

### Induction Equation - $\hat{r}$

$$-X^2 \partial_X \bar{b}_r = \frac{1}{\sin \theta} \partial_\theta (\sin \theta \bar{E}_\phi); \quad (10)$$

### Induction Equation - $\hat{\theta}$

$$-X \partial_X \bar{b}_\theta + \partial_X \bar{E}_\phi = 0; \quad (11)$$

**Induction Equation -  $\hat{\phi}$** 

$$-X\partial_X\bar{b}_\phi = \partial_X\bar{E}_\theta - \frac{1}{X}\partial_\theta\bar{E}_r, \quad (12)$$

where  $\bar{E}_r$ ,  $\bar{E}_\theta$ , and  $\bar{E}_\phi$  are related to the electric field and given by

$$\bar{E}_\phi \equiv -(\bar{W}_r\bar{b}_\theta - \bar{W}_\theta\bar{b}_r), \quad (13)$$

$$\bar{E}_\theta \equiv -(\bar{W}_\phi\bar{b}_r - \bar{W}_r\bar{b}_\phi), \quad (14)$$

$$\bar{E}_r \equiv -(\bar{W}_\theta\bar{b}_\phi - \bar{W}_\phi\bar{b}_\theta). \quad (15)$$

Finally, the 3 components of the momentum equation are given as follows:

**Momentum -  $\hat{r}$** 

$$\begin{aligned} X(\bar{W}_r + X)\partial_X\bar{W}_r + \bar{W}_\theta\partial_\theta\bar{W}_r - (\bar{W}_\theta^2 + \bar{W}_\phi^2) \\ = \frac{2\bar{p}}{\bar{\mu}} - \frac{1}{\bar{\mu}}X\partial_X\bar{p} - X\partial_X\bar{\psi} + \frac{1}{\bar{\mu}}\bar{b}_\theta\partial_\theta\bar{b}_r \\ - \frac{1}{2\bar{\mu}}X\partial_X(\bar{b}_\theta^2 + \bar{b}_\phi^2); \end{aligned} \quad (16)$$

**Momentum -  $\hat{\theta}$** 

$$\begin{aligned} X(\bar{W}_r + X)\partial_X\bar{W}_\theta + \bar{W}_\theta\partial_\theta\bar{W}_\theta + \bar{W}_r\bar{W}_\theta - \bar{W}_\phi^2 \cot\theta \\ = -\frac{1}{\bar{\mu}}\partial_\theta\bar{p} - \partial_\theta\bar{\psi} + \frac{1}{\bar{\mu}}\bar{b}_rX\partial_X\bar{b}_\theta - \frac{1}{\bar{\mu}}\bar{b}_\phi^2 \cot\theta \\ - \frac{1}{2\bar{\mu}}\partial_\theta(\bar{b}_r^2 + \bar{b}_\phi^2); \end{aligned} \quad (17)$$

**Momentum -  $\hat{\phi}$** 

$$\begin{aligned} X(\bar{W}_r + X)\partial_X\bar{W}_\phi + \frac{1}{\sin\theta}\bar{W}_\theta\partial_\theta(\sin\theta\bar{W}_\phi) + \bar{W}_\phi\bar{W}_r \\ = \frac{1}{\bar{\mu}}\bar{b}_rX\partial_X\bar{b}_\phi + \frac{1}{\bar{\mu}\sin\theta}\bar{b}_\theta\partial_\theta(\sin\theta\bar{b}_\phi). \end{aligned} \quad (18)$$

Note that the self-similar forms presented in equations 2 to 6 would represent a SIS if  $\bar{\mu} = 2$  and  $\bar{\mathbf{W}} = 0$ . A complete treatment of the self-similar problem would involve solving the  $(X, \theta)$  partial differential equations presented above, starting from a slightly perturbed SIS at some initial time  $t_0$  ( $t_0 = -\infty$  for an infinitesimal perturbation). In principle, this approach would allow us to follow the entire anisotropic development of the SIS all the way to the development of the singularity at  $t = 0$ . This could be done under various assumptions regarding the initial conditions for the rotation and magnetic field, resulting in a very complete model of protostellar collapse. This ambitious project will be left for future work. Instead, we take a more modest approach in this paper, by solving the restricted problem where all of the variables  $\bar{f}_i$  written with overbars in equations 2 to 6 can be written in the separable form

$$\bar{f}_i(X, \theta) = k_i X^{\alpha_i} f_i(\theta), \quad (19)$$

where the  $k_i$  are appropriate normalizing constants. In the case of  $\bar{\mu}$  and  $\bar{p}$  these constants are each  $4\pi$ . They are equal to  $+1$  elsewhere. The factor that depends on  $X$  is eliminated by carefully balancing powers of  $\alpha_i$ , resulting in the following system of ordinary differential equations in  $\theta$ , written here in the same order as in equations 7 to 12 and 16 to 18.

$$6\Psi + \frac{1}{\sin\theta}d_\theta(\sin\theta d_\theta\Psi) = 4\pi\mu, \quad (20)$$

$$3W_r + 2 + \frac{1}{\sin\theta}d_\theta(\sin\theta W_\theta) + W_\theta d_\theta \ln\mu = 0, \quad (21)$$

$$3b_r + \frac{1}{\sin\theta}d_\theta(\sin\theta b_\theta) = 0, \quad (22)$$

$$-2b_r + \frac{1}{\sin\theta}d_\theta[\sin\theta(W_r b_\theta - W_\theta b_r)] = 0, \quad (23)$$

$$2b_\theta - 3(W_\theta b_r - W_r b_\theta) = 0, \quad (24)$$

$$-2b_\phi + 3(W_\phi b_r - W_r b_\phi) + d_\theta(W_\phi b_\theta - W_\theta b_\phi) = 0, \quad (25)$$

$$\begin{aligned} W_r + W_r^2 + W_\theta d_\theta W_r - (W_\theta^2 + W_\phi^2) \\ = -2\frac{p}{\mu} - 2\Psi + \frac{1}{4\pi\mu}[(b_\theta d_\theta b_r - 2(b_\theta^2 + b_\phi^2)], \end{aligned} \quad (26)$$

$$\begin{aligned} W_\theta + W_\theta d_\theta W_\theta + 2W_r W_\theta - W_\phi^2 \cot\theta = -\frac{d_\theta p}{\mu} - d_\theta\Psi \\ + \frac{1}{4\pi\mu}[2b_r b_\theta - \frac{1}{2}d_\theta(b_r^2 + b_\phi^2) - b_\phi^2 \cot\theta] \end{aligned} \quad (27)$$

$$\begin{aligned} W_\phi + 2W_r W_\phi + \frac{W_\theta}{\sin\theta}d_\theta(\sin\theta W_\phi) \\ = \frac{1}{4\pi\mu}[2b_r b_\phi + \frac{b_\theta}{\sin\theta}d_\theta(\sin\theta b_\phi)]. \end{aligned} \quad (28)$$

Equations 20 to 28 are the final equations, whose solutions we study for the remainder of this paper.

The physical variables are given explicitly by the following forms, in which we have replaced  $X$  by  $r$  and  $t$ , using the definition of  $X$  given in equation 1:

$$\mathbf{v} = -\frac{r}{t}\mathbf{W}(\theta), \quad (29)$$

$$\mathbf{B} = \frac{r}{\sqrt{Gt^2}}\mathbf{b}(\theta), \quad (30)$$

$$\rho = \frac{1}{Gt^2}\mu(\theta), \quad (31)$$

$$p = \frac{1}{Gt^4}[r_0^2 p_0^* + r^2 p(\theta)] \quad (32)$$

$$\Phi = \frac{r^2}{t^2}\Psi(\theta). \quad (33)$$

Note that we have replaced the term involving  $p_0(t)$  in equation 6 with one involving only the constant  $p_0^*$ , which can be chosen *a posteriori* to keep the total pressure positive throughout the region of interest. Formally we have set  $p_0(t) = \frac{4\pi}{c_s^4 t^4} r_0^4 p_0^*$ .

One should realize that our final set of equations can also be obtained by using these physical forms directly in the equations of self-gravitating MHD, without ever writing down the  $(X, \theta)$  forms of the equations (equations 7 to 18). However, our treatment has the advantage of providing the equations within the context of a broader class of self-similarity, which may be useful for future analysis. It is important to realize that  $c_s$  has disappeared from these equations, as would any dimensional constant used in equation 1. Thus there is a “route” to these equations from quite general initial conditions, which is the main reason for our suspicion that it may be an attractor.

The nature of our model as an internal settling solution is clear from the self-similar forms in equations 29 to 33, before we even solve the equations. We observe that all velocity components go to zero proportionally to  $r$ , which also implies that there is rigid rotation on each cone defined by  $\theta = \text{const}$ . Of course, the angular velocity is allowed to vary between cones, and material flows between them.

A difficulty arises when one tries to solve the self-similar form of Poisson's equation given in equation 20. Any solution to equation 20 must satisfy the boundary conditions  $\Psi'(0) = 0$  and  $\Psi'(\pi/2) = 0$ , so that there is no  $\theta$  component of the gravitational acceleration at either boundary. The solution to the homogeneous form of the equation ( $\mu = 0$ ) which satisfies these boundary conditions, is the following:

$$\Psi_{hom} = cP_2(\cos \theta) = c\frac{1}{2}(3\cos^2 \theta - 1), \quad (34)$$

where  $P_2(\cos \theta)$  is the second order Legendre polynomial and  $c$  is an arbitrary constant. Note that the homogeneous solution, with arbitrary  $c$  may be added to any particular solution of equation 20, which produces an additional term in the gravitational acceleration. The solution to Poisson's equation is non-unique for our system, since any such solution satisfies the boundary conditions at the polar and equatorial boundaries. This non-uniqueness originates from the self-similarity. Poisson's equation has a unique solution provided that appropriate boundary conditions can be specified *everywhere* on a surface enclosing the region of interest. However, there is no unique way to specify the potential at radial infinity for our distribution of matter, which in principle extends to infinity. In practice our solution must be halted at some surface  $R(\theta, t)$  whose form depends on the matching to an external medium. The best that we can do is to limit ourselves to the special case where  $\mu(\theta)$  is constant and the density distribution is spherically symmetric at all times. In that case,  $\Psi$  should be constant on physical grounds, so that the isopotential surfaces are spherical as well. Poisson's equation (20) is then trivially solved:

$$\Psi = \frac{2}{3}\pi\mu. \quad (35)$$

We use this equation and the underlying assumptions of constant  $\mu$  and  $\Psi$  for the remainder of the analysis in this paper.

Note that the restriction that  $\mu = const$  implies a sort of "poloidal incompressibility" on our system, which takes the place of a thermodynamic equation of state (EOS) in our system, in the same way that true incompressibility replaces a thermodynamic EOS in incompressible fluid dynamics. It is generally not possible to impose any additional EOS directly relating  $p(\theta)$  to  $\mu(\theta)$  or any other variable, without imposing complete boundary conditions on Poisson's equation.

We commented in Section 2 that our solution must only be valid near the centre of a collapsing core, where the dynamical timescale is much shorter than the cooling time of the molecular gas. Realistically, our settling solution must be embedded within a nearly isothermal exterior region, which would remain nearly isothermal, as a result of the efficient cooling provided by molecular lines and the longer dynamical timescale outside of the collapsing region. The boundary joining our model to such a region would undoubtedly be complex in both shape and internal structure, with shocks arising near the outflow axis. A more complete model, which explicitly includes this external region would be very difficult to treat analytically. The equatorial region is expected to contain both accretion discs and magnetically neutral points as suggested above, while there may be more violent activity (including shocks in super Alfvénic flow) near the axes. None of this can appear in the simple asymptotic forms that

we study here. The only effect of the external region in the present calculation is through the background pressure  $p_0(t)$  in equation 32, which has no effect on the dynamics whatsoever.

The self-similar forms given by equations 29 to 33 become singular at  $t = 0$  over the entire domain of validity, and they cannot be continued beyond this singularity. This is unlike the usual point singularity (i.e. a "core" of finite mass) that forms at  $t = r = 0$  in the spherically symmetric collapse models, across which the solution may be continued into the core accretion phase. Such a solution (but with appropriate asymmetry) would be external to the solution presented here.

The inner boundary of our solution is the growing hydrostatic core and realistically, we expect the self-similar solution to vanish altogether before  $t = 0$ . This can happen if the outer boundary is shrinking in time as the inner boundary grows. We can make this plausible near the equatorial plane by observing that outside the transition region we can expect a mass flux  $\propto c_s^3/G$ , as given by Shu (1977). At the "boundary"  $R$  of our inner region equations (3) and (2) show that the mass flux scales as  $R^3/t^3$  and thus by equating the two expressions we obtain  $R \propto c_s t$ . Consequently the outer boundary of our solution may be expected to shrink onto the hydrostatic core before  $t \rightarrow 0$ , thus removing the mathematical singularity from the domain over which our solution is valid.

We turn in the next section to an analysis of these equations.

### 3 INTEGRALS

There is considerable redundancy in our equations. We note that equation 22 can be derived from equations 23 and 24 by simple algebra. There are also several integrals that can be derived from our equations. Equation 24 is already in the form of an integral. Combined with equations 22 and 21, we easily find the following two integrals, in simplified form:

$$b_\theta = qW_\theta, \quad (36)$$

$$b_r = q\left(W_r + \frac{2}{3}\right), \quad (37)$$

where  $q$  is a constant. A third integral can be obtained by inserting the first two into equations 20 to 28 and seeking a relation between  $b_\phi$  and  $W_\phi$ :

$$b_\phi = qW_\phi + \Omega \sin \theta, \quad (38)$$

where  $\Omega$  is another constant. Note that these integrals allow us to remove the self-similar magnetic field  $\mathbf{b}$  entirely from the equations to be solved.

Although it is not essential to the arguments of the present paper we might reflect a little on the general significance of these integrals. They are likely to be more general in fact than our particular solution. In their present physical form they read:

$$\begin{aligned} B_r &= \frac{q}{\sqrt{Gt}} \left( \frac{2}{3} \frac{r}{t} - v_r \right), \\ B_\theta &= -\frac{q}{\sqrt{Gt}} v_\theta, \\ B_\phi &= \frac{\Omega r \sin \theta}{\sqrt{Gt^2}} - \frac{q}{\sqrt{Gt}} v_\phi. \end{aligned}$$

If we rearrange these equations into vector form as

$$\mathbf{v} - \frac{2}{3} \frac{\mathbf{r}}{t} = -\frac{\sqrt{G}t}{q} \mathbf{B} + \frac{\Omega}{qt} \times \mathbf{r},$$

where  $\Omega$  is along the axis of symmetry, then we can recognize a kind of Ferraro's theorem (in the form  $\mathbf{v} = \text{const.} \times \mathbf{B} + \omega \times \mathbf{r}$  where  $\omega$  is the angular velocity of the field line) with time dependence. The constants are time-dependent here and the material velocity is relative to a freely-falling, zero-energy, Keplerian observer. One might expect the time dependence to be different for different self-similar symmetries.

## 4 ANALYTIC SOLUTION AND ANALYSIS

### 4.1 Boundary Conditions and Method of Solution

We now turn to the task of actually solving the self-similar equations presented in the previous section, subject to all appropriate boundary conditions. With the help of the integrals given in equations 36 to 38, equations 21 to 35 can be reduced to a system of equations involving only the self-similar velocity components  $\mathbf{W}$ , pressure  $p$ , and their derivatives with respect to  $\theta$ . Solving for the derivatives, the equations can be written as a dynamical system in standard form, which specifies a boundary value problem in four variables on the interval  $\theta \in [0, \pi/2]$ .

The boundary conditions at the symmetry axis and equatorial plane are as follows. The self-similar velocity components  $W_\theta$  and  $W_\phi$  must vanish at  $\theta = 0$ , where we also require that  $W_r > 0$  for an outflow solution. The velocity component  $W_\theta$  must vanish at the equatorial plane  $\theta = \pi/2$  for quadrupolar symmetry. The "dynamical" component of the pressure  $p$  must be negative everywhere, since the pressure would increase radially outward otherwise, according to the self-similar form for the pressure given by equation 32. The total pressure can be made positive throughout the region of interest, which is bounded on the inside by the forming hydrostatic core and on the outside by the external molecular gas that provides the source of the background pressure  $p_0(t)$  in our model. Note that we have demanded strict analyticity everywhere on the angular domain for the solutions presented in this paper. This restriction could, in principle, be relaxed by allowing a singular radial velocity along the axis, in the spirit of FH1 and LHF.

The following symmetry conditions allow us to extend our solutions from  $[0, \pi/2]$  to the full sphere  $[0, \pi]$ . Under reflection about the midplane ( $\theta \rightarrow \pi - \theta$ ), we assume that  $W_\theta \rightarrow -W_\theta$ ,  $b_r \rightarrow -b_r$ , and  $b_\phi \rightarrow -b_\phi$ . All other quantities remain unchanged upon reflection. Note that the reversal of the magnetic field at the midplane requires the existence of a current sheet in the equatorial plane, which is in accordance with the scenario discussed in Section 5 for the generation of the quadrupolar field. Note that the symmetry assumed here differs from our previous work, where we assumed that  $W_\theta \rightarrow -W_\theta$  and  $b_\theta \rightarrow -b_\theta$ , with all other quantities unchanged upon reflection. In this case, continuity requires that both  $W_\theta$  and  $b_\theta$  must vanish on the midplane, thus requiring quadrupolar symmetry for all solutions. This is *not* required in general for the present model, which admits solutions with dipolar symmetry in principle. Different equatorial boundary conditions are required, notably  $b_\theta \neq 0$  and

continuous, but this is permitted in principle by the time dependence. We will, however, concentrate on the quadrupolar class of solutions in this paper.

We proceeded first with a numerical survey of the solutions in an extended region of parameter space. However, it gradually became clear from the extremely simple appearance of the solutions and one extremely robust result (see equation 52 below), that an underlying analytical solution was at play. Once we realized this, it was relatively easy to discover the form of the analytical solution. Given the parameters  $\mu$ ,  $q$ , and  $\Omega$ , we assume a solution of the following form and solve for the constants  $c_1$  through  $c_6$  in the resulting algebraic set of equations, which are derived from the reduced system of equations involving only the self-similar velocity components and pressure:

$$W_r(\theta) = c_1 + c_2 \cos^2 \theta \quad (39)$$

$$W_\theta(\theta) = c_3 \sin(2\theta) \quad (40)$$

$$W_\phi(\theta) = c_4 \sin \theta \quad (41)$$

$$p(\theta) = c_5 + c_6 \sin^2 \theta. \quad (42)$$

After straightforward but tedious algebraic manipulations, it turns out that the constants  $c_2$  through  $c_6$  can all be expressed in terms of  $c_1$  and the other three parameters mentioned above:

$$c_2 = -2 - 3c_1 \quad (43)$$

$$c_3 = -\frac{c_2}{2} \quad (44)$$

$$c_4 = -\frac{c_2 q \Omega}{6\pi\mu(1+2c_1) + q^2 c_2} \quad (45)$$

$$c_5 = -\frac{2}{3}\pi\mu^2 - \mu(1+2c_1)(1+c_1) \quad (46)$$

$$c_6 = \frac{1}{4\pi} \left\{ -(c_4 q + \Omega)^2 + 2\pi\mu [c_4^2 - c_2(1+c_1)] \right\} \quad (47)$$

The parameter space is four-dimensional, with solutions to our boundary value problem completely specified by choosing  $\mu$ ,  $q$ ,  $\Omega$ , and  $c_1$ .

This solution clearly possesses quadrupolar symmetry, as defined above. We have checked this solution numerically for many values of the parameters. In addition, our numerical analysis did not find any other classes of solution. Thus, it appears that the analytic solution given above is the unique solution to our boundary value problem. We suspect that other classes of solutions, including singular solutions and solutions with dipolar symmetry, may exist if different boundary conditions are allowed.

Not all of the solutions given by equations 39 to 47 correspond to protostellar collapse and outflow solutions. From equation 39, we note that outflow solutions require  $c_1 < 0$  and  $c_2 > |c_1|$ , so that material falls in near the equatorial plane and is ejected near the symmetry axis. With the help of equation 43, this restriction implies that  $c_1 < -1$ . The opposite conditions provide us with solutions in which the flow is reversed, with infall near the polar axis and expulsion near the equatorial plane. The maximum value of the self-similar dynamical pressure is  $c_5 + c_6$ . Thus, we require  $c_5 + c_6 < 0$ , which keeps both the dynamical pressure and the outward pressure gradient negative, as discussed in Section 2.1. There are, in fact, solutions with  $p > 0$  so that the pressure increases with radius. Such solutions might be physically interpreted as anisotropic collapse solutions that

are driven primarily by a sudden increase in the external pressure. This sort of collapse might be reasonable in regions where star formation is initiated by a strong external shock. However, we restrict ourselves to less exotic cases in this paper, where the pressure decreases radially outward.

## 4.2 Characteristics of the Model and Exploration of the Parameter Space

In this section, we discuss the general properties of the analytical solution given by equations 39 to 47. We supplement this discussion by a rather complete exploration of the parameter space, in which we allow the parameters  $q$ ,  $\Omega$ , and  $c_1$  to vary within pre-defined ranges given by

$$\begin{aligned} 0 \leq \mu &\leq 10^3 & -10^3 \leq q &\leq 10^3 \\ -10^3 \leq \Omega &\leq 10^3 & -10^3 \leq c_1 &\leq -1. \end{aligned} \quad (48)$$

We sampled these ranges normally in each parameter  $p_i$  when  $|p_i| \leq 1$  and log-normally when  $|p_i| > 1$ . We find acceptable solutions right up to the edges of our parameter space given by equation 48. In principle, we could expand the region of our parameter space search even further than the ranges given above. However, our choice to limit our parameter space is consistent with the spirit of our self-similar analysis, where non-dimensional parameters are not usually expected to be too many orders of magnitude greater or less than unity.

The Alfvén singularity in our self-similar equations occurs when  $m_{A,\theta} = 1$ , where

$$m_{A,\theta}^2 \equiv \frac{4\pi\mu W_\theta^2}{b_\theta^2}. \quad (49)$$

Note that the usual Alfvénic singularity is modified by our self-similarity ansatz so that only the  $\theta$  components of the velocity and magnetic field are involved (eg. Tsinganos *et al.* 1996, LHF). This can be simplified with the help of equation 36:

$$m_{A,\theta}^2 = \frac{4\pi\mu}{q^2}. \quad (50)$$

The Alfvénic mach number has a constant value for each solution, which does not vary with either radius or angle. Both super-Alfvénic and sub-Alfvénic models are allowed, although there are no models where material passes through an Alfvén point. Not, however, that the special solution where  $m_{A,\theta} = 1$  everywhere is allowed. Somewhat arbitrarily, we eliminate any solution for which  $m_{A,\theta} < 0.1$ , which corresponds to magnetic energy densities in  $b_\theta$  greater than 50 times the kinetic energy density in  $W_\theta$ . This provides us with a convenient way to exclude strongly sub-Alfvénic models with unrealistically high magnetic field strengths.

There are several important conclusions that can be drawn directly from equations 39 to 47. From equation 39, and with the help of equation 44, the ratio of the outflow velocity to the infall velocity is given by

$$\frac{W_r(0)}{W_r(\pi/2)} = -2 - \frac{2}{c_1}. \quad (51)$$

The ratio  $W_r(0)/|W_r(\pi/2)| < 2$  for all models, since  $c_1$  is negative. This upper limit on the net acceleration of the gas means that the axial outflow velocity is at most twice the equatorial inflow velocity on a sphere of some given radius,

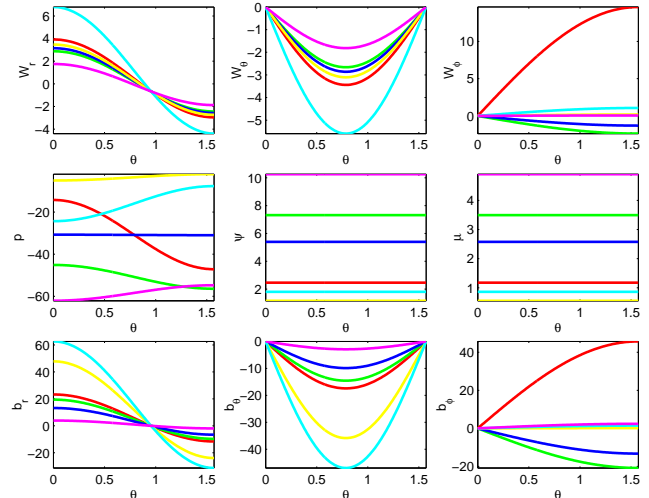


**Figure 1.** We show an overlay of 6 typical solutions. Each model is colour coded for easy comparison between panels.

at some instant of time. However, it is important to note that the velocity increases linearly with radius in our model, which is very different from the model presented in FH1, where the velocity decreases with radius as  $r^{-1/2}$ . Section 4.4 shows that any given fluid particle escapes to radial infinity along the outflow axis in the finite time required for the central singularity to develop (at  $t = 0$ ). Thus, large outflow velocities are attained at some distance from the origin, near the time when the singularity develops. Realistically, the ejected material must encounter a shock with the external region at some finite radius, where the acceleration would presumably end. Nevertheless, the possibility of a strong jet-like outflow remains, provided that the external medium is encountered at sufficient distance from the origin.

The early stage of outflow modelled in this paper is dominated by a quadrupolar circulation pattern with an outflow along the symmetry axis. It is very likely that the outflow would become even more vigorous at a later stage of evolution, in which energy is injected directly into the gas in the form of heat from the protostar. We have previously included such heating in a steady state version of our quadrupolar flow model (FH1, LHF) and found that much higher velocities can indeed be achieved. Thus, the present model might represent the immediate predecessor in the evolutionary sequence leading up to our steady-state models.

Figure 1 shows 6 of our solutions, chosen at random, overlaid on a single plot to illustrate the large dynamic range of self-similar velocities, magnetic field strengths, and pressures allowed. The curves are colour-coded for easy comparison between panels. The large allowed range of initial conditions and protostellar properties reflects the robustness of our model and of quadrupolar flow in general.

Now we examine the ratio of the radial magnetic field at the polar axis to the radial field at the equator. By combining equations 37, 39, and 44, it is easy to show that

$$\frac{B_r(0)}{B_r(\pi/2)} = -2 \quad (52)$$

for all solutions. This surprising result indicates that the flow is structured such that the radial component of the magnetic

field is always compressed to precisely the same extent. It is interesting that we first noticed this result in outflow solutions obtained numerically using a shooting code. This was one of the key results that suggested the existence of a general analytic solution to our boundary value problem, and led us to the solution presented in equations 21 to 35.

A careful examination of Figure 1 reveals that most of our models have a low pressure region near the symmetry axis, but some demonstrate the opposite behaviour. This effect can be explained by consulting equations 42, 38, 41, and 47. Note that  $c_6$  is the self-similar pressure difference between the midplane and the polar axis:

$$c_6 = p(\pi/2) - p(0). \quad (53)$$

Note also that the term  $(c_4 q + \Omega)$  in equation 47 is the maximum value of the self-similar toroidal field  $b_\phi$ . Thus, a strong toroidal field tends to make  $c_6$  negative, so that the pressure is highest at the polar axis. Clearly, this compression is due to the radial pinch of the toroidal field toward the polar axis (e.g. Fiege & Pudritz 2000a,b). On the other hand, the constant  $c_4$  in the second term is equal to the maximum rotational velocity, which acts in the opposite sense to push material away from the axis. This centrifugal barrier produces a low pressure region near the axis when the toroidal field is not sufficiently strong to counter its effect. We refer to these models as “tornado” solutions, while we often refer to  $b_\phi$  dominated models as magnetically pinched. A useful parameter to investigate these two types of behaviour is the ratio of the dynamical pressure at the the symmetry axis divided by the pressure at the midplane:

$$\frac{p(0)}{p(\pi/2)} = \frac{c_5}{c_5 + c_6}. \quad (54)$$

Since  $p < 0$ , tornado-type solutions correspond to  $p(0)/p(\pi/2) > 1$ , while magnetically pinched solutions have the opposite behaviour, with  $p(0)/p(\pi/2) < 1$ . In Figure 2, we plot this quantity against the magnetic pressure ratio  $b_r(\theta_0)^2/b_{pol}(\theta_0)^2$ , where  $b_r(\theta_0)$  and  $b_{pol}(\theta_0)$  are respectively the self-similar toroidal field and poloidal field (defined by  $b_{pol} = \sqrt{b_r^2 + b_\theta^2}$ ) components, evaluated at the angle

$$\theta_0 = \cos^{-1} \left[ \sqrt{-c_1/c_2} \right], \quad (55)$$

which divides the equatorial infall zone from the polar outflow zone (See equation 39). Since  $c_1 < -1$ , equation 43 implies that  $\theta_0$  has a maximum possible value of  $\cos^{-1} \sqrt{1/3} \approx 54.7^\circ$ . Note that the transition between tornado and magnetically pinched solutions occurs when  $b_{\phi,max}^2/b_{r,max}^2 \approx 1$ , as one would expect. It is clear from the figure that most of the parameter space is filled with solutions of the tornado type. Both super and sub-Alfvénic solutions are represented in this figure, with no apparent discontinuity in behaviour. Note the sharp boundaries that are visible in the distribution of tornado type solutions. These are due to two limits that can be shown analytically from 54, with the help of equations 46 and 47:  $p(0)/p(\pi/2) \rightarrow 4$  as  $c_1 \rightarrow -\infty$ , and  $p(0)/p(\pi/2) \rightarrow 1$  as  $\mu \rightarrow \infty$ .

It is interesting to comment on the origin of the toroidal field component in our model. The integral given in equation 38 shows that the toroidal magnetic field can be expressed as a the sum of two terms:

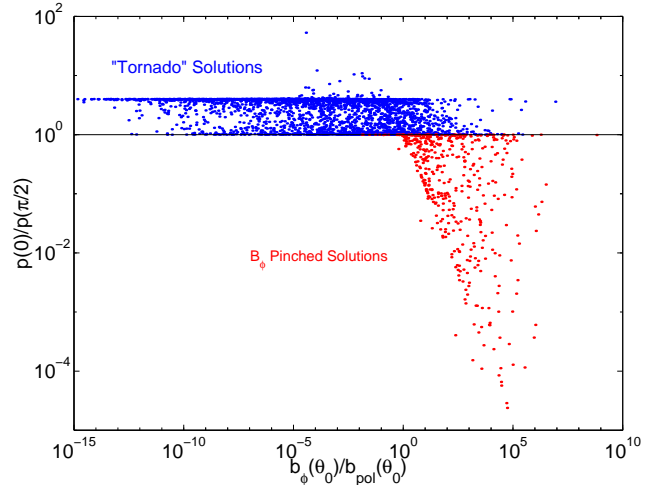


**Figure 2.** Scatter plot of the ratio of the pressure at the axis over the pressure at the midplane, as a function of  $b_{\phi,max}^2/b_{r,max}^2$  for 5000 models.  $p(0)/p(\pi/2) > 1$  corresponds to “tornado” type solutions, while  $p(0)/p(0)/p(\pi/2) < 1$  models are pinched by the toroidal magnetic field. (Recall that  $p < 0$  - see Fig. 1).

$$b_\phi = \frac{W_\phi}{W_r + 2/3} B_r + \Omega \sin \theta \quad (56)$$

The first term is associated with toroidal field generated by  $W_\phi$  twisting poloidal field lines, while the second term can be identified with toroidal flux loops simply advected by the gas motions.

### 4.3 Streamlines and Fieldlines

Figure 3 is a split-frame figure showing the instantaneous stream (right hand side) and field (left hand side) lines in the poloidal plane, overlaid with vectors whose lengths are proportional to the magnitude of the poloidal velocity or magnetic field at each point. The stream and field lines are respectively given by solutions to the differential equations

$$\frac{dr}{r d\theta} = \frac{W_r}{W_\theta} \quad (57)$$

$$\frac{dr}{r d\theta} = \frac{B_r}{b_\theta}. \quad (58)$$

It is clear from the figure that the stream and field lines in the poloidal plane are not parallel. The stream and field lines are superimposed over a colour representation of the pressure on the left, and the toroidal field strength on the right.

The path traced out by a fluid element in a time dependent model may not coincide with the instantaneous streamlines because the streamlines themselves evolve in time. However, an interesting property of our self-similar model is that a given fluid element followed in time actually obeys equation 57, and hence moves only along the instantaneous streamlines. This behaviour arises because time enters into each velocity component with the same power in equation 29, and the components of  $\mathbf{W}$  do not explicitly depend on time. Thus the streamlines in the left panel of Figure 3 can also be interpreted as the paths of individual fluid elements.

Figure 4 shows a three-dimensional representation of a

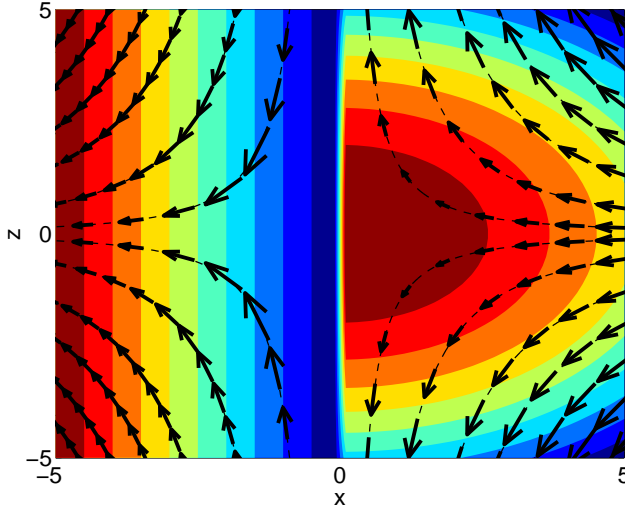


**Figure 3.** We show poloidal field lines (left) and streamlines (right) for a typical solution. These are overlaid on a colour plot of the toroidal field ‘pressure’  $b_\phi^2/8\pi$  on the left, and the gas pressure on the right. This particular model is a ‘tornado’ type solution. The parameters of the model shown are as follows:  $\mu = 1.77$ ,  $q = -6.11$ ,  $\Omega = -14.56$ ,  $c_1 = -4.33$ .

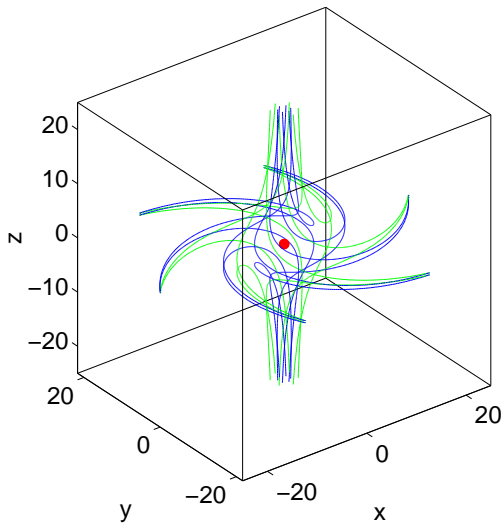


**Figure 4.** We show a three-dimensional view of several streamlines (blue) and field lines (green). Note that there is considerable rotation in flow, and that the streamline and field lines are not parallel, indicating the presence of a Poynting flux. The model shown is the same as the one in Figure 3.

several stream and field lines equally spaced in angle and reflected about the midplane. We have selected a model with a significant amount of rotation for this figure, whose parameters given in the caption of figure 3). The stream and field lines wrap around the origin as pressure gradients deflect the material out along the symmetry axis. Note the similarity to the corresponding plot (Figure 5) in FH1.

#### 4.4 The Trajectories of Fluid Elements

Some additional insight into the flow structure can be obtained by directly integrating the trajectories followed by fluid elements. It is trivial to integrate equation 40, with the help of equation 29, to show that

$$\frac{\tan \theta}{\tan \theta_0} = \left( \frac{t}{t_0} \right)^{-2c_3}, \quad (59)$$

where  $\theta_0$  is the poloidal angle of a fluid particle at some initial time  $t_0 < 0$ . Combining equations 43 and 44, we find that

$$c_3 = \frac{2 + 3c_1}{2} < -1/2 \quad (60)$$

since  $c_1 < -1$  for all outflow solutions (Refer to the discussion following 47). Thus, all fluid elements with  $\theta_0 < \pi/2$  go to the symmetry axis  $\theta = 0$  when the central density becomes singular at  $t = 0$ . Fluid elements on the asymptotic streamline that starts at  $\theta_0 = \pi/2$  go to the origin at  $t = 0$ . Note that an initially spherical shell of fluid is transformed by the flow into an thin ‘needle-like’ distribution of material along the symmetry axis.

It is also possible to obtain an exact expression for the radial part of the trajectory by directly integrating equation 57, using the forms given in equations 39 and 40. We find that

$$\frac{r}{r_0} = \left( \frac{\tan \theta}{\tan \theta_0} \right)^{c_1/(2c_3)} \left[ \left( \frac{\sin \theta}{\sin \theta_0} \right) \left( \frac{\cos \theta_0 + 1}{\cos \theta + 1} \right) \right]^{c_2/(2c_3)}. \quad (61)$$

Therefore,  $r \propto \theta^{(c_1+c_2)/(2c_3)}$  near the time  $t = 0$ , when  $\theta \rightarrow 0$ . The discussion following equation 47 demonstrated that  $c_1 + c_2 > 0$  for all outflow solutions, and equation 60 indicates that  $c_3 < 1$ . Thus, we find the intriguing result that material escapes to infinity for all outflow solutions in the finite time required for the the central singularity to develop. This confirms that our model can indeed generate strong, jet-like outflows, provided that they can escape to sufficiently large distances before encountering a shock with the external medium.

## 5 DISCUSSION

In this section, we deal mainly with the question of where the preceding solution may be expected to apply. The reader may find it helpful to refer to Figure 5 throughout this discussion, where we provide a sketch of the magnetic field configuration that we describe below.

We proceed first with a qualitative discussion. For simplicity, we assume that the magnetic and angular momentum axes of a cold cloud core coincide. The collapse of a molecular core may be due to the inside-out collapse of a SIS (Shu 1977; GS), albeit one that is threaded by a magnetic field. Alternatively, it may be due to the loss of magnetic support due to ambipolar diffusion, or due to the damping of Alfvén waves or MHD turbulence. The collapse might even result from the arrival of a sudden shock or torsional Alfvén wave (Habé *et al.* 1991). Whatever the cause of the collapse, it is likely that a nearly radial magnetic field develops during collapse, as the field lines are dragged in with the collapsing gas. These radial field lines will be oppositely directed across the equatorial plane. It is in this plane (presumably

near the Keplerian point where the gas velocity may be relatively slow compared to the magnetic diffusion speed) that one can expect the central magnetic field to disconnect from the external field through the formation of an X type neutral point near the equator (e.g. Shu et al. 1994). The field lines should remain roughly radial outside of the equatorial X points, especially near the midplane, as illustrated in Figure 5.

We must, however, also consider the pressure driven bounce of material in opposite directions above and below the equator along the axis. This rebounding material forms a quadrupolar velocity field (FHI; Tomisaka, 1998; LHF), which distorts the radial field locally into rising axisymmetric poloidal arches if the flow is super-Alfvénic. As usual there will also be a toroidal component of the magnetic field in these arches. These arches will also advect the toroidal component of the field with the rising gas. The key point is that these arches should develop first at small radii, where we expect the most vigorous bounce. Ultimately, we expect this flow pattern to lead to the formation of quadrupolar velocity and magnetic fields consistent with the field structure that we have assumed in this series of papers. However, a full quantitative analysis remains to be done. The arches may themselves reconnect sporadically (through the formation of toroidal X lines), if the gas has finite resistivity so that ideal MHD does not strictly apply. This would have the effect of producing magnetic toroids looped around the axis, which would rise with the mean flow velocity. After each such disruption the persistent quadrupolar flow should reestablish the quadrupolar field. These magnetic ejections may be associated with the production of energetic particles and hence “flaring” (e.g. Montmerle *et al.* 2000 for the detection of significant X-ray emission from class I protostars), and are probably of interest in their own right as features in the bipolar outflow.

The solution presented in this paper applies at smaller radii than the radius of the outer X point. As we have discussed above, the bounce at this outer point is created by a mixture of rotational-magnetic support and radiative heating (e.g. LHF), whereas the bounce at the inner X point is caused by the forming hydrostatic core. At this inner X point, we expect a transition to a dipolar magnetic field (although a quadrupolar circulation may still be present). Note that our equations may admit dipolar solutions, which could apply to the hydrostatic core at very small radii. However, we have not yet found any such solutions. Thus the settling solution that we have presented here is expected to lie between inner and outer X points. Near the equator the field lines are actually wrapped around a magnetic O point. This equatorial XOX configuration may be a quite general magnetic structure necessary to the process of star formation. It links the outer “Keplerian” disc to a more slowly growing inner hydrostatic core. The core probably grows to become the star at the expense of the O-type envelope.

One can also get some feeling for the applicability of our solution by looking at some numerical relations. We can rewrite equation (31) to give  $t = -\sqrt{(\mu/G\rho)}$  which shows that  $\sqrt{\mu}$  gives the time before the final singularity in units of the (approximate) free-fall time. Let us suppose that the region in which we are interested extends inward from about 1 au to the boundary of the hydrostatic core. If this region has a mass  $m$  in solar mass units then

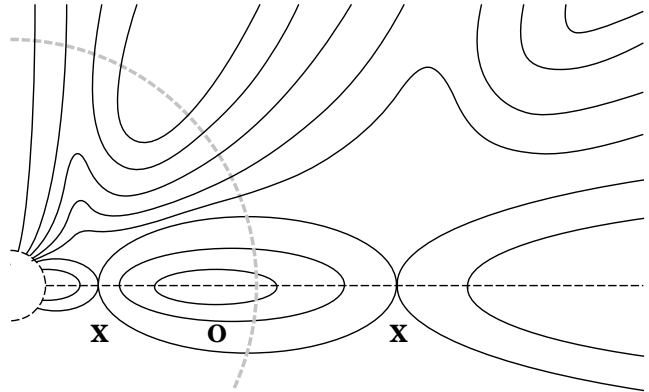


**Figure 5.** We sketch the possible regions where quadrupolar stream and field lines may arise during the formation of a star. The solution presented in this paper is concerned with the inner region while that presented in our earlier papers concerns the outer region.

$\rho \approx 2m \times 10^{-7} g \text{ cm}^{-3}$ . Using  $m = 0.1M_\odot$  for a low mass star, we arrive at  $t \approx \sqrt{\mu}$  years. From equations (29) and the solution (39), we see that the inward equatorial velocity at 1 au is about  $4c_1/\sqrt{\mu} \text{ km s}^{-1}$ . Therefore if  $c_1 = -c\sqrt{\mu}$  where  $c$  is of order one but is sufficiently large to make  $p < 0$  (see equation 42), then the bipolar velocity approaches  $8c \text{ km s}^{-1}$  and the equatorial velocity is comparable to the free fall velocity.

It is also of interest to consider the magnitude of the magnetic field in this illustration. At 1 au the equation (30) plus the solution and our preceding assignments of the constants gives the equatorial radial field to be of order 100 gauss. Of course this ignores the total magnetic field which is a bit more difficult to estimate because of the  $\phi$  component and its relation to the rotation of the system. Note that these numbers are provided for illustrative purposes only. Our models admits a large range of solutions that can describe a variety of protostellar objects.

## 6 CONCLUSIONS AND SUMMARY

We have developed a new model for the time dependent and anisotropic collapse that occurs within the inner regions of a star-forming molecular cloud core. By including the effects of self-gravity and MHD, our model provides a reasonably complete description of the dynamics on all scales between the inner hydrostatic core and an outer X point. Our previous steady-state version of the model is expected to apply external to the collapsing region modelled here, and possibly at later times. Remarkably, the collapse model presented in this paper admits an exact and completely analytic solution. We note that there are few other analytic solutions of this complexity in all of MHD. We summarize our solution here, for the reader’s convenience:

$$v_r = -\frac{r}{t}(c_1 + c_2 \cos^2 \theta) \quad (62)$$

$$v_\theta = -\frac{r}{t}[c_3 \sin(2\theta)] \quad (63)$$

$$v_\phi = -\frac{r}{t}(c_4 \sin \theta) \quad (64)$$

$$P = \frac{r_0^2}{Gt^4} p_0^* + \frac{r^2}{Gt^4} [c_5 + c_6 \sin^2 \theta] \quad (65)$$

$$\rho = \frac{1}{Gt^2} \mu, \quad (66)$$

$$B_r = \frac{r}{\sqrt{Gt^2}} \left[ q(c_1 + c_2 \cos^2 \theta + \frac{2}{3}) \right], \quad (67)$$

$$B_\theta = \frac{r}{\sqrt{Gt^2}} qc_3 \sin(2\theta) \quad (68)$$

$$B_\phi = \frac{r}{\sqrt{Gt^2}} (qc_4 + \Omega) \sin \theta \quad (69)$$

$$\Phi = \frac{2}{3} \pi \frac{r^2}{t^2} \mu, \quad (70)$$

where the four free parameters of the model are  $\mu$ ,  $q$ ,  $\Omega$ , and  $c_1$ . The remaining constants in these expressions are given by equations 43 to 47. Note that the time  $t$  starts large and negative, and the model evolves until a central singularity forms at  $t = 0$ .

The main point of this work is to demonstrate that infall and outflow can coexist and arise naturally from our self-similar equations, with few additional assumptions. The outflow that arises is surprisingly vigorous, despite the lack of explicit internal heating in our model. We find that the outflow velocity increases linearly with radius, and that material in the outflow escapes to radial infinity in the finite time required for the central singularity to develop. More realistically, we expect the outflow to interact with the surrounding gas, outside of the self-similar region. This would limit the velocity of the outflow, but high velocities could still be obtained if the shock occurs much further out than the radius from which the material originated.

Our model applies only at intermediate scales between two X type magnetic neutral points. We expect a transition to a dipolar field internal to the inner X point, where the growing hydrostatic protostellar core resides. This region could, in principle, be modelled using the same set of equations we have used in the protostellar collapse region modelled here, with boundary conditions consistent with a dipolar field. The region exterior to the outer X point is probably characterized by longer dynamical timescales than the protostellar collapse region. Once the overall quadrupolar flow structure is established by the collapse, the outer region might be most appropriately modelled by the steady-state (or perhaps quasi-steady) version of this model, which we have previously discussed in depth (FH1, LHF). Future work on this class of models may proceed in two alternate directions. We may try to join together the three regions discussed above, in piecewise fashion, to provide a more complete description of the simultaneous infall and outflow processes. Alternatively, we might turn to the more ambitious problem of solving the most general self-similar partial differential equations given in Section 2.1 (equations 7 to 18) over the entire range of scales.

## 7 ACKNOWLEDGEMENTS

This project was supported by a CITA/NSERC postdoctoral fellowship (JDF), an operating grant from NSERC (RNH), and by the combined support of NSF Grant AST-0978765 and the University of Rochester's Laboratory for Laser Energetics (TL). A preliminary account of this work

was presented at the Cracow meeting on "Plasma Turbulence and Energetic Particles in Astrophysics" (1999, M. Ostrowski and R. Schlickeiser, eds.). In addition, the authors would like to thank an anonymous referee for an exceptionally thorough review, which helped us to strengthen our paper substantially.

## REFERENCES

Aburihan M., 1999, Masters Thesis, Queen's University  
 Aburihan M., Henriksen R.N., 1999, *ptep.proc.*, 339  
 André P., Ward-Thompson, D., Barsony, M., 1993 *ApJ*, 406, 122  
 André P., Montmerle, T., 1994, *ApJ* 420, 837  
 Basu S., 1997, *ApJ* 485, 240  
 Basu S., Mouschovias T.C., 1995, *ApJ* 452, 386  
 Basu S., Mouschovias T.C., 1995, *ApJ* 453, 271  
 Bertout C., 1989, *ARA&A* 27, 351  
 Carter, B., Henriksen, R.N., 1991, *J. Math. Phys.* 32, 10, p.2580  
 Fiege, J.D., Henriksen, R.N., 1996, *MNRAS* 281, 1038  
 Fiege J.D., Pudritz R.E., 2000, *ApJ* 534, 291  
 Fiege J.D., Pudritz R.E., 2000, *MNRAS* 311, 85  
 Fiege J.D., Pudritz R.E., 2000, *MNRAS* 311, 105  
 Foster P.N., Chevalier R.A., 1993, *ApJ* 416, 303  
 Galli D., Shu F.H., 1993, *ApJ* 417, 220  
 Habe A., Uchida Y., Ikeuchi S., Pudritz R.E., 1991, *PASJ*, 43, 703  
 Henriksen, R.N., Valls-Gabaud, D., 1994, *MNRAS* 266, 681  
 Henriksen, R.N., Andre P., Bontemps S., 1997, *A&A* 323, 549  
 Hunter C., 1977, *ApJ* 218, 834  
 Larson R.B., 1969, *MNRAS* 145, 271  
 Lery T., Henriksen R.N., Fiege J.D., 1999, *A&A*, 350, 254  
 Li Z., Shu F.H., 1996, *ApJ* 472, 211  
 Montmerle T., Grosso N., Tsuboi Y., Koyama K., 2000, *ApJ* 532, 1097  
 Myers P.C., Ladd E.F., Fuller G.A., 1991, *ApJ* 372L, 95  
 Penston M.V., 1969, *MNRAS* 144, 425  
 Ryden B.S., 1996, *ApJ* 471, 822  
 Shu F.H., 1977, *ApJ* 214, 488  
 Shu F.H., Najita J., Ostriker E., Wilkin F., Ruden S. and Lizano S., 1994, *ApJ* 429, 781  
 Tomisaka, K., 1998, *ApJ* 502L, 163  
 Whitworth A., Summers D., 1985, *MNRAS* 214, 1